Retrieval of birefringent and scalar pupils from stacks of blurred point-spread functions generated by fluorescent nanobeads

R. Gutiérrez-Cuevas[1, 2, *] and L. A. Alemán-Castañeda[1]

[1] *Aix Marseille Univ, CNRS, Centrale Marseille, Institut Fresnel, UMR 7249, 13397 Marseille Cedex 20, France*

[2] *Institut Langevin, ESPCI Paris, Université PSL, CNRS, 75005 Paris, France*

(Dated: April 21, 2023)

Here we present the theory and the different strategies for retrieving the pupil of in fluorescence microscopy where the effects of birefringence play an important role. We also study the effect of separating the signal into different polarization channels.

I. INTRO

General intro about fluorescence microscopy, SMOLM and PSF engineering. Finish by saying something along the lines of: However, any aberration or misalignment in the system can affect the final shape of the PSFs and thus lead to an inaccurate estimate of the parameters.

A common solution to this problem is to perform a set of calibration measurements with a known source and at varying focal planes [1, 2]. From these measurements and an accurate model for the propagation of the light emitted by the source to the camera, the aberrations can be estimated through phase retrieval algorithms. Initially, only scalar models with point sources were used which allowed the successful use of both iterative and nonlinear optimization routines for estimating the aberrations [1–3]. However, more accurate models [4, 5] take into account the vectorial nature of light which is essential to describe the propagation of the emitted radiation through the interface between the suspension medium and the immersion liquid used for the high-NA microscope objective [6]. Moreover, it is also necessary to consider that the most common sources, such as fluorescent nanobeads, emit incoherent light and their size can thus lead to a noticeable blurring of the PSFs. Given these more accurate assumptions, iterative algorithms cannot be directly applied and have to be adapted which can make them unstable, although some success has been demonstrated [4]. A more natural approach is to use nonlinear optimization [5, 7] since it provides us with the freedom to incorporate other unknown parameters into the estimation, such as the photobleaching amplitudes or the background illumination.

Up until now, all works have assumed a scalar pupil to characterize the aberrations or to design new PSFs. However, SMOLM requires the use of birefringent elements to encode the orientation information of the emitting dipole into the shape of the two polarization components of the PSF. Therefore, it is important to update the model of propagation for an accurate characterization or design of SMOLM systems. In this work, we propose a characterization technique and algorithm to estimate the polarization aberrations of the system [8] as well as other unknown (or poorly known) parameters. This is done by applying a nonlinear optimization algorithm to a physical model where the aberrations (or widow we want to design) are now represented by a Jones matrix. The implementation is done with the neural network framework `PyTorch` [] which performs automatically all the gradient computation []. Additionally, we show that, in general, it is necessary to introduce polarization diversity in the measurements in order to properly characterize the polarization response. This is similar to the introduction of phase diversity by taking images at various focal planes. Additionally, we implement the most useful method for taking into account the blurring to the size of the nanobead discussed in []. It should also be noted that all the results obtained in this work were achieved with the software `torchPSFstack` which is freely accessible at [].

II. MODELING THE PSFS FOR FLUORESCENCE MICROSCOPY

A. Field at the back-focal plane

The first step is to have the most accurate model for the propagation of light through our microscope. As shown in Fig. 1, the source is embedded in a medium of index of refraction n_i at a distance z_0 from the interface with immersion oil of index of refraction n_f, the interface is given by the coverslip which is assumed to be index matched to the immersion oil. For a dipolar source, the green tensor at the back-focal plane (BFP) of a high-NA objective can be computed through Richards-Wolf diffraction theory for aplanatic systems [6**?**]. An important step in this calculation is to take into account the interface between the two media since it introduces spherical aberration and the coupling of evanescent waves when $n_f > n_i$, known as supercritical angle fluorescence (SAF), which can contribute to more than half of the radiation reaching the detector [9–11].

Following [6, 12] and assuming that light propagates along the positive $\hat{z}$ direction, the Green tensor at the

* rodrigo.gutierrez-cuevas@fresnel.fr

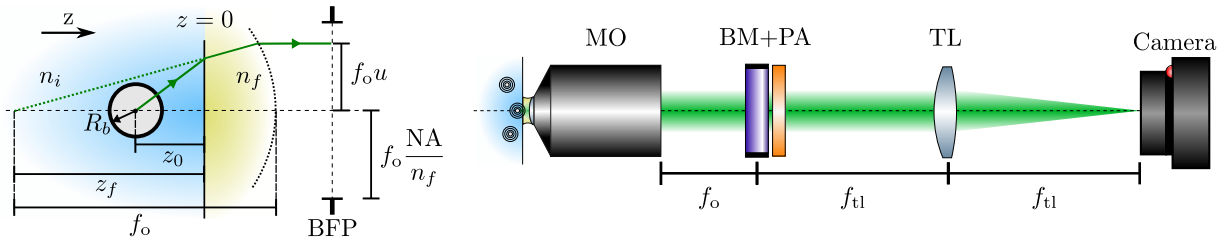

FIG. 1. Schematic of the experimental setup for the collection and shaping of the emission by a source. (left) Schematic of the position source, in this case represented by a fluorescent nanobead, with respect to the interface between the embedding medium of index of refraction n_i with the immersion medium of index of refraction n_f used for the high-NA microscope objective and of the focal plane. (right) Schematic of the collection arm composed of a microscope objective (MO), followed by a birefringent mask (BM) and a polarization analyzer (PA). The light at the BFP is then focused onto the camera by the tube lens of focal length f_{tl}.

BFP,

$$\mathbf{G}(\mathbf{u};\mathbf{r}_0) = e^{-\mathrm{i}kn_f\boldsymbol{\rho}_o\cdot\mathbf{u}} \exp\left[\mathrm{i}kn_i|z_0|\sqrt{1-\left(\frac{n_f u}{n_i}\right)^2}\right] \times \exp\left(\mathrm{i}kn_f z_f\sqrt{1-u^2}\right)\mathbf{g}(\mathbf{u}), \quad (1)$$

where

$$\mathbf{g}(\mathbf{u}) = \begin{pmatrix} g_{xx}(\mathbf{u}) & g_{xy}(\mathbf{u}) & g_{xz}(\mathbf{u}) \\ g_{yx}(\mathbf{u}) & g_{yy}(\mathbf{u}) & g_{yz}(\mathbf{u}) \end{pmatrix} \quad (2)$$

with the explicit form of its components given in the Appendix, $\mathbf{r}_0 = \boldsymbol{\rho}_0 + \hat{\mathbf{z}}z_0$ is the position of the source with $\boldsymbol{\rho}_0 = (x_0, y_0)$ denoting its transverse location, $k = 2\pi/\lambda$ with λ being the wavelength, and z_f is the location of the focal plane from the interface, $z_f < 0$ ($z_f > 0$) if the focal plane is in the medium with index of refraction n_i (n_f). The vector $\mathbf{u} = (u_x, u_y)$ denotes the normalized coordinates at the BFP, see Fig. 1. The maximum value of $u = \|\mathbf{u}\|$ is limited by the NA through $u_{\max} = \mathrm{NA}/n_f$. The matrix elements g_{ij} include the effect of the Fresnel coefficients of the boundary and depend on $\mathbf{u}$ but not on the location of the dipole or the focal plane. For a dipole oriented along the unit vector $\boldsymbol{\mu} = (\mu_x, \mu_y, \mu_z)$, the electric field distribution at the BFP is given by

$$\mathbf{E}(\mathbf{u};\mathbf{r}_0) = \mathbf{G}(\mathbf{u};\mathbf{r}_0)\cdot\boldsymbol{\mu}. \quad (3)$$

Therefore, the three columns of the Green tensor represent the field distribution produced by a dipole along each of the three coordinate axes.

B. Propagation from the BFP to the image plane

In order to encode information about the position and orientation of the dipole into the shape of the PSF, it is necessary to include a mask into the path of the emitted light at the BFP with the possible help a relay system as shown in Fig. 1. The most general case is that of a birefringent mask represented by a 2×2 Jones matrix [],

$$\mathbf{J}_{\mathrm{M}}(\mathbf{u}) = \begin{pmatrix} J_{xx} & J_{xy} \\ J_{yx} & J_{yy} \end{pmatrix}. \quad (4)$$

Note that a scalar mask case with apodization is regained if $q_j = 0$ for $j = 1,2,3$, and a pure phase mask if also $q_0 = 1$. After multiplying the Green tensor by this Jones matrix, the field can then be propagated form the BFP to the image plane through

$$\mathbf{G}_{\mathrm{IP}}(\tilde{\boldsymbol{\rho}};\mathbf{r}_0) = \iint \mathbf{J}_{\mathrm{M}}(\mathbf{u})\cdot\mathbf{G}_0(\pm\mathbf{u},;\mathbf{r}_0)e^{-\mathrm{i}k\frac{n_f\tilde{\boldsymbol{\rho}}}{M}\cdot\mathbf{u}}\mathrm{d}\mathbf{u}, \quad (5)$$

where $\tilde{\boldsymbol{\rho}}$ denotes the transverse position at the image plane, and M is the total magnification of the system. Note that the normalized coordinate is defined at the location of the birefringent mask. Assuming an incoherent source, the PSF is then given by

$$I_{\mathrm{IP}}(\tilde{\boldsymbol{\rho}};\mathbf{r}_0) = \|\mathbf{G}_{\mathrm{IP}}\|^2 = \sum_{i=x,y}\sum_{j=x,y,z}|G_{\mathrm{IP},ij}(\mathbf{u})|^2. \quad (6)$$

III. MODELING FOR THE PHASE RETRIEVAL

A. Polarization aberrations

The decomposition of polarization aberrations by a Jones matrix can be done in the following manner

$$\mathbf{J}_{\mathrm{A}}(\mathbf{u}) = e^{\mathrm{i}2\pi W(\mathbf{u})}\begin{pmatrix} q_0(\mathbf{u})+\mathrm{i}q_3(\mathbf{u}) & q_2(\mathbf{u})+\mathrm{i}q_1(\mathbf{u}) \\ -q_2(\mathbf{u})+\mathrm{i}q_1(\mathbf{u}) & q_0(\mathbf{u})-\mathrm{i}q_3(\mathbf{u}) \end{pmatrix}, \quad (7)$$

which allows separating the scalar aberrations, contained in W from the vectorial correction given by the q's. Since aberrations tend to be described by smooth functions, it generally suffices to decompose the various elements of the Jones matrix using the Zernike polynomials which constitute a complete basis on the unit disk. Therefore, we write

$$W(\mathbf{u}) = {\sum_l}' c_l^{(W)} Z_l(\mathbf{u}/u_{\max}), \quad (8)$$

$$q_j(\mathbf{u}) = \sum_l c_l^{(j)} Z_l(\mathbf{u}/u_{\max}), \quad (9)$$

where $j = 0, ..., 3$, and we used a single index notation for the basis. Note that $\sum'$ in the expression for W indicates that the terms corresponding to piston and defocus should be excluded, this is automatically handled by the software []. The piston term only fixes a global phase which cannot be determined from intensity measurements while the defocus term is redundant with the more accurate defocus parameter z_f in Eq. 1. From now on, it will be assumed that the source is placed along the optical axis so that $\boldsymbol{\rho}_0 = (0, 0)$, with any deviation from this being corrected be the scalar tilts present in W.

This Zernike expansion is inspired by the Nijboer-Zernike theory [13–15] where a scalar mask would be separated into real and imaginary parts before decomposing in terms of Zernike polynomials. Note that other models can be used, such as pixel by pixel decomposition, but a Zernike decomposition with enough terms should be able to handle most cases found in microscopes. Moreover, computationally there is no advantage to considering a pixel decomposition since the number of DFT (the most costly operation) would be the same. It should also be noted that a scalar mask can easily be modeled by just setting the coefficients $c_l^{(j)} = 0$ for all l and $j = 1, 2, 3$.

B. Best focus and the distance to the coverslip

In general the position chosen as the nominal focus (or best focus) z_f and distance to the coverslip of the emitter z_0 are not perfectly known. Therefore, it is worth considering them as part of the optimization parameters that will be estimated along with the coefficients of the Zernike decomposition of the birefringent mask. The most obvious solution is to directly use z_f and z_0 as parameters, however both phase terms have similar effect when the radial coordinate u is below the SAF radiation which might cause the nonlinear optimization to fall into a local minimum. Therefore, it is best to consider instead

$$\mathbf{G}(\mathbf{u}) = D_{\delta,\Delta z_f}(\mathbf{u})\mathbf{g}(\mathbf{u}), \tag{10}$$

where

$$D_{\delta,\alpha}(\mathbf{u}) = \exp\left\{\mathrm{i}2\pi n_f \delta\left[\frac{n_i}{n_f}\sqrt{1-\left(\frac{n_f u}{n_i}\right)^2} - \alpha\sqrt{1-u^2}\right]\right\} \tag{11}$$

$$\times \exp\left(\mathrm{i}2\pi n_f \Delta z_f \sqrt{1-u^2}\right), \tag{12}$$

with $\delta = |z_0|/\lambda$ and $z_f = \Delta z_f - \alpha|z_0|$. The key difference is that α is a constant that is chosen to minimize root-mean squared wavefront error (or a similar metric) over the range $u \in [0, n_i/n_f]$. The parameter δ now predominantly controls the amount of exponential decay for the SAF radiation while Δz_f controls the defocus of the system. The plane $\Delta z_f = 0$ is where the spherical aberration induced by the interface is best compensated with a simple defocus. Nonetheless, this plane might not coincide with the nominal focal plane chosen during the experimental acquisition given that the choice of the best focus from the image on the camera is quite subjective. In the supplemental document, we provide common choices for the best focus with the appropriate PSF for various distances to the coverslip. These can be used to determine a better initial value for $Deltaz_f$ by comparing them to the data acquired experimentally.

Even though this new choice of parameters helps the algorithm to differentiate between the two effects, if some apodization is included in the model then this can mimic or compensate for the exponential decay controlled by δ. Therefore, on must be careful when including δ in the optimization routine. For fluorescent nanobead samples it is safe to assume that they are all fixed to the coverslip so that their distance to the coverslip can be taken as their radius and thus δ can be taken off the optimization routine. Nonetheless, in all the numerical experiments a slight error (chosen randomly between 0 and 20nm) was introduced for the value of z_0, this error did not affect the final estimation of the pupil.

C. Phase and polarization diversity

In phase retrieval algorithms for optical microscopes, it is common practice to assume that we have access to a stack of intensity images at varying focal distances separated by Δz_ζ from the location of the best focus. This varying focal distances are taken into account by multiplying the Green tensor by the phase factor

$$D^\zeta(\mathbf{u}) = \exp\left[\mathrm{i}kn_f \Delta z_\zeta \sqrt{1-u^2}\right] \tag{13}$$

This additional information, referred to as phase diversity, helps the algorithm converge to an appropriate solution without falling into local minima and helps discriminate between the right and left phase vortices. These measurements are sufficient when the aberrations are taken as scalar, however when birefringence effects need to be taken into account it is necessary to implement a method to also provides information about the polarization state of the PSFs for each focal distance. This supplementary information can be obtained by inserting a polarization analyzer right after the birefringence mask (see Fig. 1). This polarization analyzer can be composed of a combination of waveplates and polarizers where at least one element can rotate in order to change the polarization projection of the output. This polarization diversity is modeled by a set of constant Jones matrices $\mathbf{P}^{(p)}$ that is applied after all other birefringent masks. Therefore, the stack of Green tensors at the BFP is given by

$$\mathbf{G}_{\mathrm{BFP}}^{(\zeta,p)}(\mathbf{u}) = D^{(\zeta)}(\mathbf{u})\mathbf{P}^{(p)} \cdot \mathbf{J}_{\mathrm{A}}(\mathbf{u}) \cdot \mathbf{J}_{\mathrm{M}}(\mathbf{u}) \cdot \mathbf{G}_0(\mathbf{u}). \tag{14}$$

In this model $\mathbf{J}_{\mathrm{M}}$ represents any known birefringent mask into the nominal Green tensor which can have approximately known parameters that can be incorporated into

the optimization routine. It is worth noting that while experimentally the polarization diversity happens at the BFP, computationally it is better to perform it at the image plane in order to avoid the computation of unnecessary DFTs.

D. Modeling the total measured intensity

To model the intensity measured by the camera, the Green tensor is first propagated to the image plane via,

$$\mathbf{G}_{\mathrm{IP}}^{(\zeta,p)}(\boldsymbol{\rho}) = \iint \mathbf{G}_{\mathrm{BFP}}^{(\zeta,p)}(\mathbf{u}) e^{-\mathrm{i}k\frac{n_f\boldsymbol{\rho}}{M}\cdot\mathbf{u}} \mathrm{d}\mathbf{u}. \tag{15}$$

Here, it will be assumed that the source emits fully unpolarized light. This is the case for fluorescent nanobeads which are commonly used to characterize or test fluorescence microscopes since they have a stronger signal than that emitted by single fluorescent molecules. In this case the measured intensity is given by the incoherent sum of the PSFs produced by dipoles oriented along each of the three Cartesian axes which is the same as the squared Frobenius norm of the Green tensor at the image plane

$$I_{\mathrm{IP}}^{(\zeta,p)}(\boldsymbol{\rho}) = \left\| \mathbf{G}_{\mathrm{IP}}^{(\zeta,p)} \right\|^2 = \sum_{i=x,y} \sum_{j=x,y,z} |G_{\mathrm{IP,ij}}^{(\zeta,p)}(\mathbf{u})|^2. \tag{16}$$

Depending on the size of the source it might be necessary to perform one of the blurring operations described in []. If a three-dimensional blurring is needed the computation of supplementary quantities will need to added to the forward model, for example, for the exact hard-sphere model we would also need to compute the total intensity for other values of $d_c s$. The downside is that this would slow the algorithm considerably. However, as long as their diameter is smaller than 30nm one can safely skip this step. More details about the blurring models implemented can be found in the Supplementary Information.

As a last step for computing the measured intensity, we also consider the effect of photobleaching of the fluorescent nanobeads and the background illumination. The photobleaching causes the number of photons emitted by the nanobead to diminish with time. Its effect can be taken into account by implementing an overall amplitude factor $\mathcal{A}^{(p,\zeta)}$ which depends on both the phase and polarization diversities. The background illumination is then added incoherently to the photobleached PSF stack. The simplest model is to assume that the background illumination is constant across each intensity image and determined by the term $\mathcal{B}^{(p,\zeta)}$. Therefore, the final total measured intensities of the ZP stack are given by

$$I_{\mathrm{tot}}^{(\zeta,p)}(\boldsymbol{\rho}) = a^{(p,\zeta)} I_{\mathrm{IP}}^{(\zeta,p)}(\boldsymbol{\rho}) + b^{(p,\zeta)}. \tag{17}$$

It is possible to assume a more complicated model for the background illumination, such as a quadratic expansion [16].

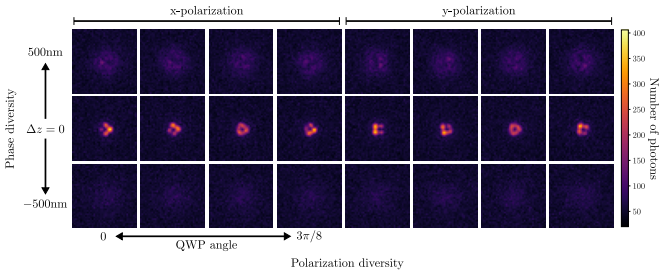

FIG. 2. PSF stack with phase and polarization diversities modelled with `pyPSFstack` and used for the retrieval of the Jones matrix of an SEO element.

E. Cost function

The last piece we need to consider is the choice of a cost function that compares how good our modeled PSFs $I_{\mathrm{tot}}^{(\zeta,p)}$ are compared to the measured ones $I_{\mathrm{exp}}^{(\zeta,p)}$. Under the absence of noise, any choice of cost function that has a minimum when the two quantities are the same should provide the same result. However, noise is ever present in experimental measurements and thus needs to be taken account. If the noise in the camera follows a Poisson distribution then the log-likelihood cost function,

$$\mathcal{C}_{\mathrm{LL}} = \sum_{\zeta,p} \iint w(\boldsymbol{\rho}) \left\{ I_{\mathrm{exp}}^{(\zeta,p)}(\boldsymbol{\rho}) \log \left[I_{\mathrm{tot}}^{(\zeta,p)}(\boldsymbol{\rho}) \right] - I_{\mathrm{tot}}^{(\zeta,p)}(\boldsymbol{\rho}) \right\} \mathrm{d}^2\boldsymbol{\rho}. \tag{18}$$

Whereas if it follows a Gaussian distribution then the sum of the squared difference is the most appropriate,

$$\mathcal{C}_{\mathrm{SS}} = \sum_{\zeta,p} \iint w(\boldsymbol{\rho}) \left[I_{\mathrm{exp}}^{(\zeta,p)}(\boldsymbol{\rho}) - I_{\mathrm{tot}}^{(\zeta,p)}(\boldsymbol{\rho}) \right]^2 \mathrm{d}^2\boldsymbol{\rho}. \tag{19}$$

A window function w has been introduced to represent the use of a finite region at the image plane and to exclude bad pixels if there are any. It is also worth making a technical note. In order for the choice of cost function to make sense we need to use as $I_{\mathrm{exp}}^{(\zeta,p)}$ the values that actually follows the assumed distribution. In general this means that the images should not be denoised and that the offset of the camera should be removed. A detailed description for the forward model can be found in the Supplementary Information as well as other considerations that need to be taken into account before launching the optimization routine.

IV. NUMERICAL EXPERIMENTS

To exemplify the implementation of the phase retrieval algorithm, two main birefringent masks will be considered: (2) a stress-engineered optical (SEO) element [] and (3) an s-plate [**?**]. Both have been used in practice to measure the position and orientation of dipolar emitters []. All the modelled data stacks are computed using

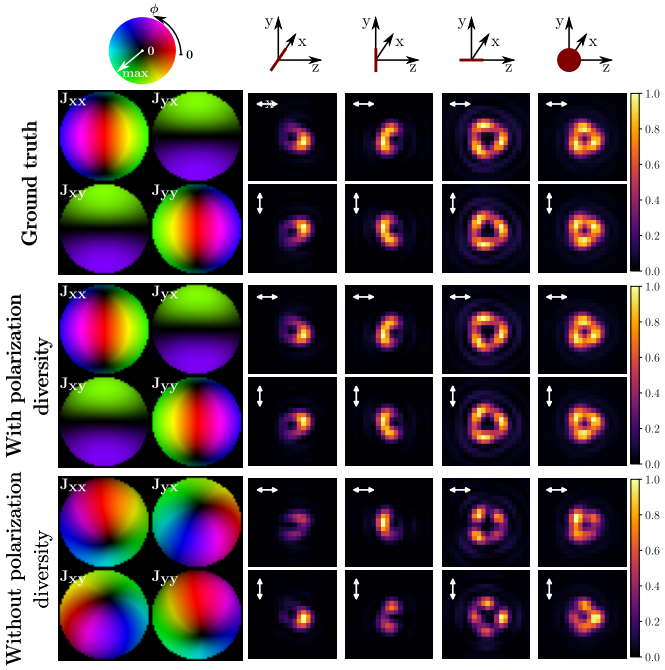

FIG. 3. .

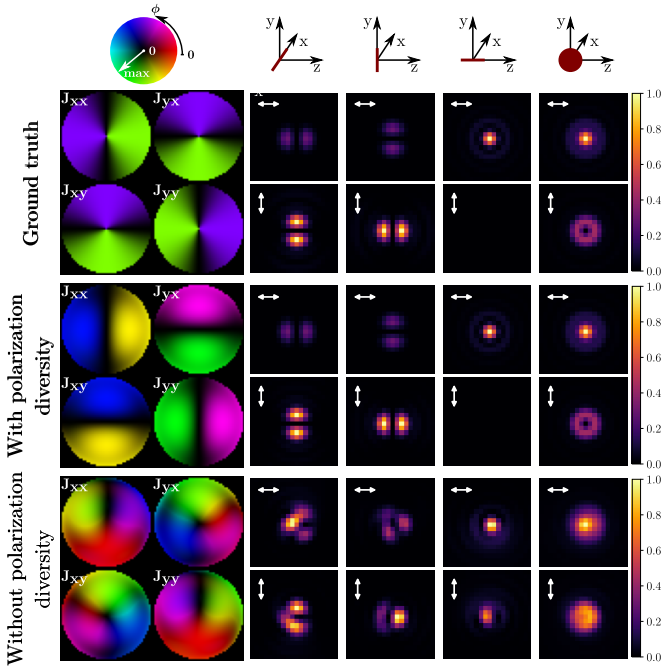

FIG. 4. .

`pyPSFstack` which allows computing the PSF stack with phase and polarization diversities, and can compute the three-dimensional blurring due to the size of the fluorescent nano-bead. Figure 2 shows as an example the stack used for retrieving the SEO birefringent mask with both phase and polarization diversity. It can also simulate the effect of the background illumination and noise. The polarization diversity will be taken as the Jones matrix given by a quarter-wave plate at various angles followed by a horizontal or vertical linear polarizer. This choice is inspired by the setup used in [] where the SEO is followed by a quarter-wave plate and then a Wollaston prism separates the two linearly-polarized components.

A. Polarization diversity VS more phase diversity

As a first example, we consider the retrieval of a birefringent mask with and without the use of polarization diversity. For this, the data is modelled assuming the source is a 20nm fluorescent nanobead, with an average of 20000 photons hitting our detectors per PSF to which we add 100 photons per pixel as the background illumination. Noise following a Poisson distribution is then added to the images. Note that the average number of photons on the PSFs measured with polarization diversity is halved due to the presence of a linear polarizer. Under these conditions, an image defocused by more than 500nm past the nominal focal plane will be indistinguishable from noise (see Fig. 2). Therefore, for the phase diversity images are taken from -500nm to 500nm of the nominal focal plane with a step size of 100nm. For the polarization diversity, the quarter wave-plate is rotated from 0 to $3\pi/8$ with a step of $\pi/8$ and is then followed by a Wollaston prism which projects into horizontal and vertical polarization.

The results of the characterization are shown in Figs. 3 and 5. These figures show the true Jones matrix along with the ones retrieved with and without polarization diversity, additionally they show the PSFs formed by dipoles oriented along the three Cartesian axes and an incoherent one. The PSFs shown are modelled according to the standard configuration for each birefringent mask, that is, for the SEO a QWP at 45° is placed after the mask and then a Wollaston prism projects onto the two linearly-polarized components while for the s-plate only the Wollaston prism is used. The need to use polarization diversity to characterize birefringent masks becomes then evident, in both cases the retrieved pupil and the corresponding PSFs are quite different from the true ones when no polarization diversity is used whereas an accurate result is achieved in the other case. It is worth commenting on the differences between the true Jones matrix for the s-plate and the one retrieved with polarization diversity. The deviation at the center comes from the model that was chosen, since the s-plate is singular at the origin the Zernike polynomials struggle to reproduce this, nonetheless the corresponding PSFs are indistinguishable from the true ones. The other noticeable difference is that the phase between the two columns is not the right one (they are $\pi/2$ out of phase). This error can happen when the birefringent mask is real up to a global phase, since the resulting PSFs look the same and therefore the algorithm cannot distinguish between the two.

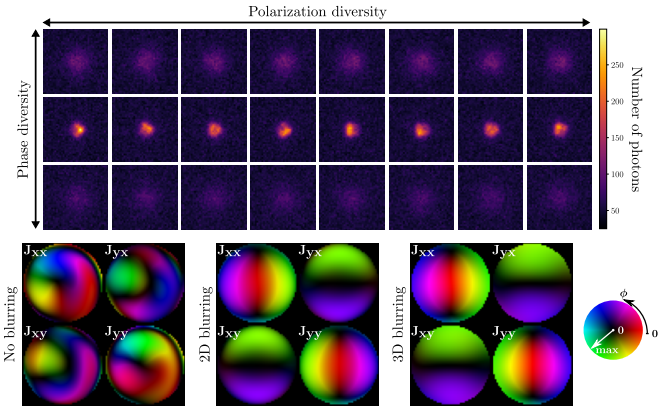

FIG. 5. .

B. Incorporating blurring due to size to the pupil retrieval

In order to showcase the implementation of blurring in our model, we now consider a 200nm fluorescent nanobead which produces blurred PSFs due to its size. Let us only treat the SEO birefringent mask with the same choice of phase and polarization diversities as before.

V. CHARACTERIZING THE POLARIZATION ABERRATIONS IN AN EXPERIMENTAL SETUP

ACKNOWLEDGMENTS

S. Paine for useful discussions.

Appendix A: Expressions for the Green tensor at the BFP

As outlined in [6], a closed-form for the Green tensor at the BFP for a dipolar source placed close to an interface can be obtained. In particular the components of the **g** tensor in Eq. (**??**) are given by

$$\mathbf{g}(\mathbf{u}) = \frac{1}{(1-u^2)^{1/4}} \begin{pmatrix} \cos^2\phi\sqrt{1-u^2}\Phi_2 + \sin^2\phi\Phi_3 & \cos\phi\sin\phi(\sqrt{1-u^2}\Phi_2 - \Phi_3) & -u\cos\phi\Phi_1 \\ \cos\phi\sin\phi(\sqrt{1-u^2}\Phi_2 - \Phi_3) & \sin^2\phi\sqrt{1-u^2}\Phi_2 + \cos^2\phi\Phi_3 & -u\sin\phi\Phi_1 \end{pmatrix}. \tag{A1}$$

where

$$\Phi_1(u) = t^p(u)\frac{n_i k_i\sqrt{1-u^2}}{n_m\sqrt{k_m^2 - k_i^2u^2}} \tag{A2a}$$

$$\Phi_2(u) = t^p(u)\frac{n_i}{n_m} \tag{A2b}$$

$$\Phi_3(u) = t^s(u)\frac{k_i\sqrt{1-u^2}}{\sqrt{k_m^2 - k_i^2u^2}} \tag{A2c}$$

with

$$t^s(u) = \frac{2k_{m,z}}{k_{m,z} + k_{i,z}}, \tag{A3a}$$

$$t^p(u) = \frac{n_m}{n_i}\frac{2n_i^2k_{m,z}}{n_i^2k_{m,z} + n_m^2k_{i,z}}. \tag{A3b}$$

being the Fresnel coefficients for p and s polarized light.

[1] B. M. Hanser, M. G. L. Gustafsson, D. A. Agard, and J. W. Sedat, Optics Letters **28**, 801 (2003).
[2] B. M. HANSER, M. G. L. GUSTAFSSON, D. A. AGARD, and J. W. SEDAT, Journal of Microscopy **216**, 32 (2004).
[3] N. A. Clark, *Microscope Characterization using Phase Retrieval Applied to Determine the Spatial Distribution of Membrane-Associated Proteins in Hematocytes*, Ph.D. thesis, University of Rochester (2012).
[4] N. H. Thao, O. Soloviev, and M. Verhaegen, Journal of the Optical Society of America A **37**, 16 (2019).
[5] B. Ferdman, E. Nehme, L. E. Weiss, R. Orange, O. Alalouf, and Y. Shechtman, Optics Express **28**, 10179 (2020).
[6] L. Novotny and B. Hecht, *Principles of Nano-Optics* (Cambridge University Press, 2006).
[7] J. R. Fienup, Applied Optics **21**, 2758 (1982).
[8] E. W. Hansen, in *Polarization Considerations for Optical*

Systems, edited by R. A. Chipman (SPIE, 1988).
[9] E. H. Hellen and D. Axelrod, Journal of the Optical Society of America B **4**, 337 (1987).
[10] D. Axelrod, Traffic **2**, 764 (2001).
[11] D. Axelrod, Biophysical Journal **104**, 1401 (2013).
[12] M. A. Lieb, J. M. Zavislan, and L. Novotny, Journal of the Optical Society of America B **21**, 1210 (2004).
[13] A. J. E. M. Janssen, Journal of the Optical Society of America A **19**, 849 (2002).
[14] J. J. M. Braat, P. Dirksen, A. J. E. M. Janssen, and A. S. van de Nes, Journal of the Optical Society of America A **20**, 2281 (2003).
[15] J. J. Braat, P. Dirksen, A. J. Janssen, S. van Haver, and A. S. van de Nes, Journal of the Optical Society of America A **22**, 2635 (2005).
[16] A. Aristov, B. Lelandais, E. Rensen, and C. Zimmer, Nature Communications **9** (2018), 10.1038/s41467-018-04709-4.